

# Geophysical Research Letters®



## RESEARCH LETTER

10.1029/2022GL101170

### Key Points:

- An inverse correlation was observed between eruption frequency and ground surface deformation of Sakurajima volcano
- Beneath the crater, muon imaging visualized that the mass density increased during ground inflation and decreased during ground deflation
- Plugging of the conduit with dense, stiff magma during recharge caused inflation during quiescent periods

### Supporting Information:

Supporting Information may be found in the online version of this article.

### Correspondence to:

L. Oláh,  
[olah.laszlo@wigner.hu](mailto:olah.laszlo@wigner.hu)

### Citation:

Oláh, L., Gallo, G., Hamar, G., Kamoshida, O., Leone, G., Llewellyn, E. W., et al. (2023). Muon imaging of volcanic conduit explains link between eruption frequency and ground deformation. *Geophysical Research Letters*, 50, e2022GL101170. <https://doi.org/10.1029/2022GL101170>

Received 7 SEP 2022  
Accepted 22 DEC 2022










### Author Contributions:

**Conceptualization:** László Oláh, Edward W. Llewellyn, Hiroyuki K. M. Tanaka  
**Data curation:** László Oláh  
**Formal analysis:** László Oláh, Osamu Kamoshida, Shouhei Ohno  
**Funding acquisition:** Gergő Hamar, Hiroyuki K. M. Tanaka, Dezső Varga  
**Investigation:** László Oláh, Gergő Hamar, Gábor Nyitrai, Takao Ohminato, Hiroyuki K. M. Tanaka, Dezső Varga  
**Methodology:** László Oláh  
**Project Administration:** Hiroyuki K. M. Tanaka, Dezső Varga  
**Software:** László Oláh, Osamu Kamoshida, Shouhei Ohno

© 2023. The Authors.

This is an open access article under the terms of the [Creative Commons Attribution License](#), which permits use, distribution and reproduction in any medium, provided the original work is properly cited.

## Muon Imaging of Volcanic Conduit Explains Link Between Eruption Frequency and Ground Deformation

László Oláh<sup>1,2</sup> , Giuseppe Gallo<sup>2,3</sup> , Gergő Hamar<sup>2,4</sup> , Osamu Kamoshida<sup>2,5</sup>, Giovanni Leone<sup>2,6</sup> , Edward W. Llewellyn<sup>7</sup> , Domenico Lo Presti<sup>2,3,8</sup> , Gábor Nyitrai<sup>2,4,9</sup> , Takao Ohminato<sup>1</sup>, Shouhei Ohno<sup>5</sup>, Hiroyuki K. M. Tanaka<sup>1,2</sup> , and Dezső Varga<sup>2,4</sup> 

<sup>1</sup>Earthquake Research Institute, The University of Tokyo, Tokyo, Japan, <sup>2</sup>International Virtual Muography Institute, Global, Tokyo, Japan, <sup>3</sup>Department of Physics and Astronomy “E. Majorana”, University of Catania, Catania, Italy, <sup>4</sup>Institute for Particle and Nuclear Physics, Wigner Research Centre for Physics, Budapest, Hungary, <sup>5</sup>NEC Corporation, Tokyo, Japan, <sup>6</sup>The University of Atacama, Copiapó, Chile, <sup>7</sup>Department of Earth Sciences, Durham University, Durham, UK, <sup>8</sup>National Institute for Nuclear Physics, Catania, Italy, <sup>9</sup>Faculty of Natural Sciences, Budapest University of Technology and Economics, Budapest, Hungary

**Abstract** Understanding the physical mechanism of ground deformation at a volcano supports the use of deformation data as a monitoring tool. An inverse correlation was observed between eruption frequency and ground deformation of Sakurajima volcano from November 2018 to April 2021. Over the same period, the mass density of magma in the conduit was monitored via muography. Mass density increased during inflation, when eruption frequency was low, and decreased during deflation, when eruption frequency was high. Periods of low eruption frequency are associated with the formation of a dense plug in the conduit, which we infer caused the inflation of the edifice by trapping pressurized magmatic gas. Conversely, periods of high eruption frequency are associated with the absence of the plug, which we infer allows gas to escape, leading to deflation. Muography thus reveals the in-conduit physical mechanism for the observed correlation, with implications for interpretation of deformation at other volcanoes.

**Plain Language Summary** The ground surface of a volcano often deforms before an eruption. Remote sensing of ground movements could be a valuable tool for eruption forecasting if the physical causes of ground deformation were known. We have used naturally occurring cosmic muons to image the changes in mass density over time in the upper plumbing system of Sakurajima Volcano (Japan) and compared this with ground surface motions and eruption activity. We found that the mass density increased during dormant periods, when the ground surface of the volcano was high, and the mass density decreased during periods of frequent eruption, when the ground surface was low. Muon imaging helped to reveal the hidden volcanic processes: the volcano plugged with dense magma during dormant periods allowing pressure in the conduit to build up, resulting in the uplift of the volcano's surface. During periods of eruption, the plug was destroyed and replaced with fresh, lower-density magma, releasing pressure and causing the volcano's surface to move downwards.

## 1. Introduction

Forecasting the location, onset, cessation, and style of impending volcanic eruptions facilitates effective mitigation of the impact of associated hazards (Poland & Anderson, 2020; Sparks, 2003). Active volcanism is driven by the subsurface evolution and movement of magmatic materials, which may induce seismicity (Breniguer et al., 2008; Chouet, 1996; Dempsey et al., 2020), ground deformation (Biggs et al., 2014, 2016), gas emission (Fischer et al., 1994; Werner et al., 2013), and fumarolic activity (Francis et al., 1980). Monitoring of the signals induced by these phenomena is indirect and interpretation of the origin of the signals is challenging because a wide variety of factors influence the behavior of magma and host rock in the run-up toward eruption (Caricchi et al., 2014; Melnik & Sparks, 2002; Woods & Koyaguchi, 1994). The occurrence of non-volcanic processes also induce changes in the monitoring signals (e.g., tectonic changes result in ground-surface deformations), thus the interpretation of monitoring signals typically relies on correlation, rather than causation. This hinders the detection and interpretation of pre-eruptive phenomena (Sano et al., 2015) and may result in “false positives”: activity that is interpreted as a precursor, which does not foreshadow an eruption (Syahbana et al., 2019). The observed

**Visualization:** László Oláh  
**Writing – original draft:** László Oláh  
**Writing – review & editing:** László Oláh, Giuseppe Gallo, Giovanni Leone, Edward W. Llewellyn, Domenico Lo Presti, Hiroyuki K. M. Tanaka

correlations between monitoring signals and eruptive activity would be more robust if they could be linked via the casual physical mechanism.

Near-real-time observations of ground surface deformations have revealed both subsidence of volcanic edifices during eruption (Massonnet et al., 1995) and inflation of volcanic edifices during quiescent periods preceding an eruption (Patané et al., 2003). Such data sets have provided insights into how edifice deformation is linked to volcanism (Biggs et al., 2014; Pinel et al., 2014). For instance, Biggs et al. (2014) present a probabilistic analysis of interferometric synthetic aperture radar data collected at 198 volcanoes over an 18-year period, which showed that 94% of the volcanoes that did not deform also did not erupt, whereas 46% of volcanoes that deformed also erupted (tectonic changes induced the remaining deformations). Modeling of magma flow and viscosity changes and pressure changes occurring in the upper part of conduit have been used to link short-term eruptive cycles to observed ground deformations, but the outcomes are not always predictable (Albino et al., 2011). Combining ground deformation measurements with other sensitive techniques can help us to understand the causal physical mechanism by which ground deformation and volcanic activity are linked, and lead toward more robust and predictive interpretations of the monitoring signals. Geophysical monitoring of combined magma and host rock mass density can reveal the underlying physical mechanism of volcanic activity by providing indirect information about the composition and spatio-temporal evolution of magma propagation to the surface (Londoño & Kumagai, 2018; Poland & Carbone, 2016). Here we use muon imaging to determine changes in mass density in the plumbing system of Sakurajima volcano (Kyushu, Japan) at a spatial resolution of a few tens of meters, on monthly basis, and relate the results to observations of both ground deformation and eruptive activity.

Eruptions at Sakurajima are dominantly vulcanian, comprising impulsive explosions that typically last minutes-to-hours (Iguchi et al., 2008; Miwa & Toramaru, 2013; Yokoo et al., 2013). Activity is cyclic, with typical inter-eruption interval of a few days (Gabellini et al., 2022). Since 2006, eruptive activity at Sakurajima has alternated between the Minamidake crater and the Showa crater (Japan Meteorological Agency, 2022). Periods of relatively high eruption frequency at a particular crater alternate with periods of quiescence—both periods typically last for several months. The physical mechanism for the hours-to-days cycles of Vulcanian explosions has been extensively investigated through analysis of visual observations, seismic and geodetic data, gas geochemistry data, and characterization of eruption products (Gabellini et al., 2022; Iguchi et al., 2008; Miwa & Toramaru, 2013; Yokoo et al., 2013). The prevailing physical model infers the presence of a dense plug of viscous magma in the upper few tens of meters of the conduit, beneath which a pressurized pocket of gas accumulates, which is a few hundred meters in vertical extent; explosions result from failure of the plug (Gabellini et al., 2022; Iguchi et al., 2008; Kazahaya et al., 2016; Miwa & Toramaru, 2013; Yokoo et al., 2013). Similar mechanisms have been invoked to explain Vulcanian activity at other volcanoes, including Semeru (Java, Indonesia), Suwanosejima (Kyushu, Japan), and Soufrière Hills (Montserrat, West Indies) among others (Burgisser et al., 2011; Iguchi et al., 2008; Watt et al., 2007). The longer-term cycles of alternating periods of high and low eruption frequency have received much less attention. Gabellini et al. (2022) study the morphological and petrological characteristics of ash emitted during Vulcanian activity at Sakurajima, and conclude that the dense, viscous plug forms over a period of several months, characterized by quiescence or low eruptive frequency, and is progressively destroyed during periods of high eruption frequency. In this work, we use muography to investigate these longer cycles.

## 2. Methodology

Muography exploits naturally occurring cosmic-ray muons to reconstruct the average densities along the paths of muons across large-scale structures, producing muon “radiographic” images (Tanaka et al., 2007). The constant flux and the high penetration power of muons allow passive and remote imaging of the shallow density structures in volcanoes at a spatial resolution of few meters (Macedonio et al., 2022; Miyamoto et al., 2022; Nishiyama et al., 2014; Oláh et al., 2018). Muography has already been used to image the spatio-temporal evolution of magmatic materials—for example, ascent and descent of magma within a volcanic vent (Tanaka et al., 2014), magma degassing (Tanaka et al., 2009), and plug formation underneath deactivated craters (Oláh et al., 2019)—and to observe structural changes (Lo Presti et al., 2022; Tioukov et al., 2022) and hydrothermal activities (Gibert et al., 2022) in volcanic systems. The early warning capabilities of muography have also been studied (Leone et al., 2021; Nomura et al., 2020; Oláh & Tanaka, 2022a). We conducted muography of Sakurajima volcano over the period from September 2018 to July 2021.

The elevation map of the observational site and schematic drawing of the experimental configuration are shown in Figure 1. We applied the Multi-Wire Proportional Chamber-based Muography Observation System (MMOS) (Oláh et al., 2018; Varga et al., 2020, 2022) of Sakurajima Muography Observatory for muographic monitoring of mass density changes underneath the active craters (Text S1 in Supporting Information S1). The small black rectangle shows the location of the observatory (O) at latitude 31.557°N and longitude 130.650°E, at altitude 150 m above sea level. The MMOS was oriented toward the active craters at 30.25° from north (defined as  $\tan(\theta_x) = 0$ ), as shown by the black arrow, and set to horizontal (defined as  $\tan(\theta_y) = 0$ ). The MMOS collected muon tracks within  $\pm 505$  mrad in the horizontal direction and  $\pm 353$  mrad in the vertical direction. The points M, S, and R were selected on the northeast slope of the volcano to extract three cross-sections across Minamidake crater, Showa crater, and Reference region, respectively. Figure 1b shows the three selected cross-sections along the OM (dark-blue-colored), OS (green-colored), and OR (yellow-colored) lines. The targeted region underneath the active crater is shown within the OP and OQ (black) lines. We note that the vertical angle region of 0–150 mrad (see under the OP line) was also covered by the MMOS, but the excessive (>2.5 km) rock thickness did not allow us to measure the density in this angular region beneath the crater. The MMOS measured the muon tracks continuously from January 2017 with only a few technical stops of a few days each during installation of new MMOS modules or maintenance work (Oláh et al., 2019, 2021; Varga et al., 2020). Upgrading the MMOS allowed to observe muons across the upper plumbing system of the Minamidake crater and monitor the changes in mass density through this region which was not yet possible in our earlier work (Oláh et al., 2019).

Data analysis relied on the methodology developed by Oláh et al. (2019). The data from the MMOS were processed to create muographic images that show the density structure through the crater region of Sakurajima volcano. Muographic images use the natural coordinate system of the MMOS that is the tangents of the projections of incoming muon directions with respect to the orientation of MMOS:  $\tan(\theta_x)$  and  $\tan(\theta_y)$  (Text S1 in Supporting Information S1). Each muographic image was captured with  $33 \times 33$  angular bins with a size of 0.023 (that corresponds to a spatial resolution of approx. 60 m at the crater, which is located at a distance of 2.65 km from the MMOS) in both horizontal and vertical directions. Each image was determined for a period of 5 months. The muographic image processing was based on comparison of modeled and measured muon fluxes. The measured trajectories of particles were reconstructed by 1+1-dimensional line fits onto coordinates on the tracking layers (Oláh et al., 2018), and the fluxes were calculated for each angular bin by taking into account the measurement time, dead time, and detector geometry (Oláh et al., 2019). Quality assurance of the data was performed by off-line analysis and low-quality data were removed from the analyzed data sets. The modeled fluxes were determined by integrating the differential muon spectra (Tang et al., 2006) from the threshold energies that were required for muons to penetrate through the volcanic edifice. Improving on the earlier work (Oláh et al., 2019), threshold energies were calculated by taking into account the stochastic energy loss processes of muons (Lipari & Stanev, 1991) via Monte Carlo simulation instead of using an analytical approach based on the continuous slowing down approximation (Groom et al., 2002). Here GEANT4 framework (Agostinelli et al., 2003) was used to simulate the energy deposit of muons in silicon dioxide and parametrize the threshold energies as a function of thickness (Oláh et al., 2021).

### 3. Results

Figure 2a–2x show images selected for the crater region with  $9 \times 5$  angular bins from a period between November 2018 and March 2021. The black line visualizes the shape of the crater along the AB line of Figure 1a. Black rectangular outlines highlight a region underneath the active Minamidake crater (M), a region underneath the dormant Showa crater (S), and a Reference region (R) through the southern flank of the volcanic edifice in which volcanism does not occur. Each selected region has the same lithology (Geological Survey of Japan, 2013). The vertical range of these regions corresponds to the angular region between the OP and OQ (black) lines in Figure 1b. The path-averaged densities ( $\rho$ ) ranged between 0.8 and 1.8 g cm<sup>-3</sup> through the regions underlying Minamidake crater and Showa crater. Density values ranged from 0.8 to 1.25 g cm<sup>-3</sup> through the Reference region. The lower densities through the Reference region likely arise because energetic (> 1 GeV) muons scattered into the MMOS from the surface of the downward sloping parts of volcanic edifice (Ambrosino et al., 2015). The white-shaded regions correspond to angular bins without density values (Figures 2a–2g, 2p–2t) due to the thickness that was not penetrated by muons during the data collection time. The muographic images show that the densities change over time through the region underneath the craters.

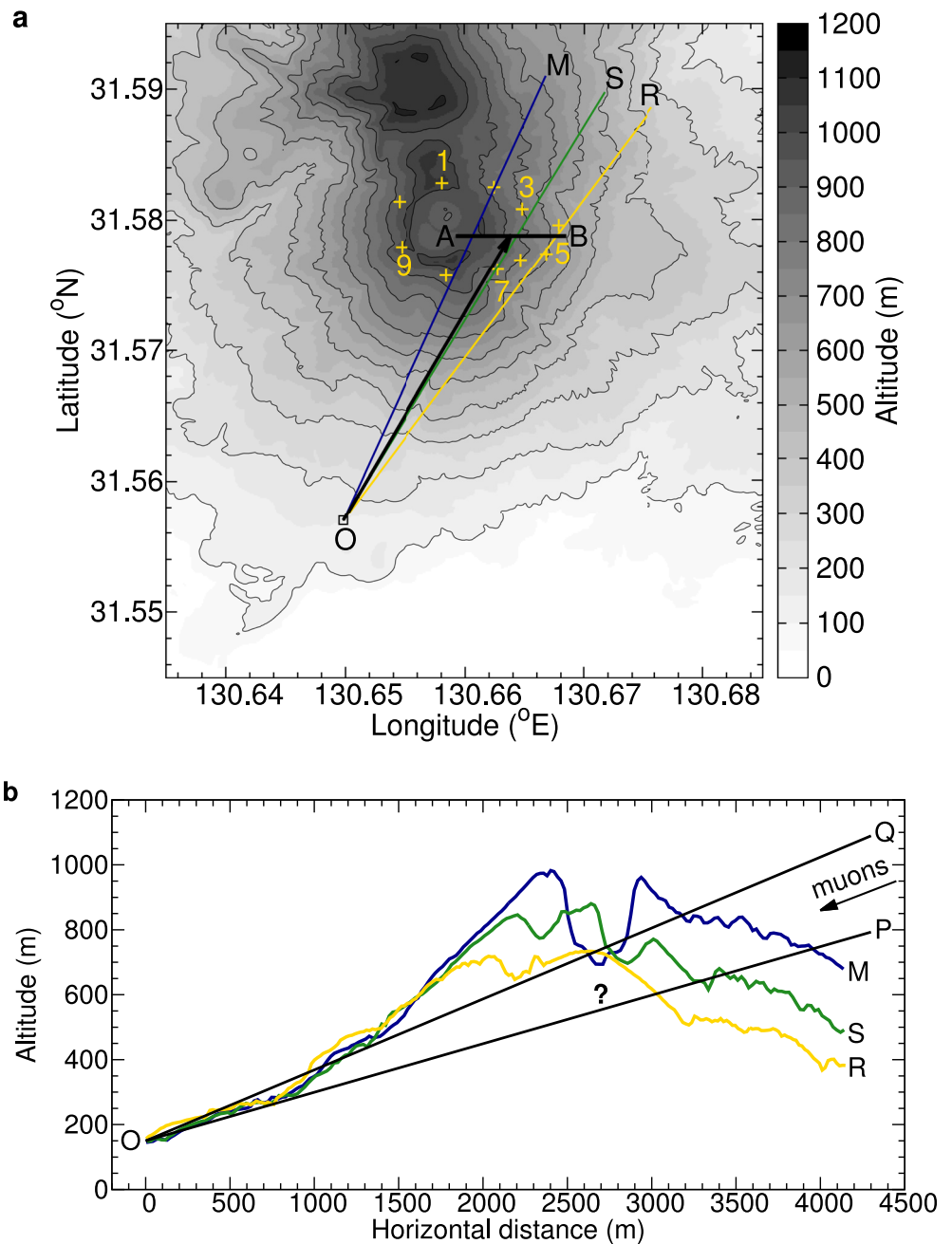


**Figure 1.** Map of measurement site and schematic of the experimental arrangement. (a) The map of Sakurajima volcano is drawn based on the digital elevation data of Geospatial Information Authority of Japan (<http://www.gsi.go.jp/>). A small black rectangle shows the location of the muography observatory (O) at latitude 31.557°N and longitude 130.650°E, at 150 m altitude above sea level. The black arrow shows the azimuthal orientation of MMOS that was set to 30.25° from north (defined as  $\tan(\theta_x) = 0$ ). The MMOS was oriented horizontally (defined as  $\tan(\theta_y) = 0$ ). OM (dark-blue-colored), OS (green-colored), and OR (yellow-colored) lines highlight three selected cross-sections across the Minamidake crater, Showa crater, and a Reference region, respectively. The AB line shows a selected cross-section across the crater region. Yellow-colored crosses and numbers (only odds are shown) refer, respectively, to the locations and identification numbers of selected sites where ground displacements were determined from the data collected by synthetic aperture radar. (b) Three cross-sections of the measurement site are shown along the OM (dark-blue-colored), OS (green-colored), and OR (yellow-colored) lines, respectively. The OP and OQ (black) lines bound the vertical range of the studied region beneath the craters. Question mark shows the location of volcanic conduits within the studied angular region.

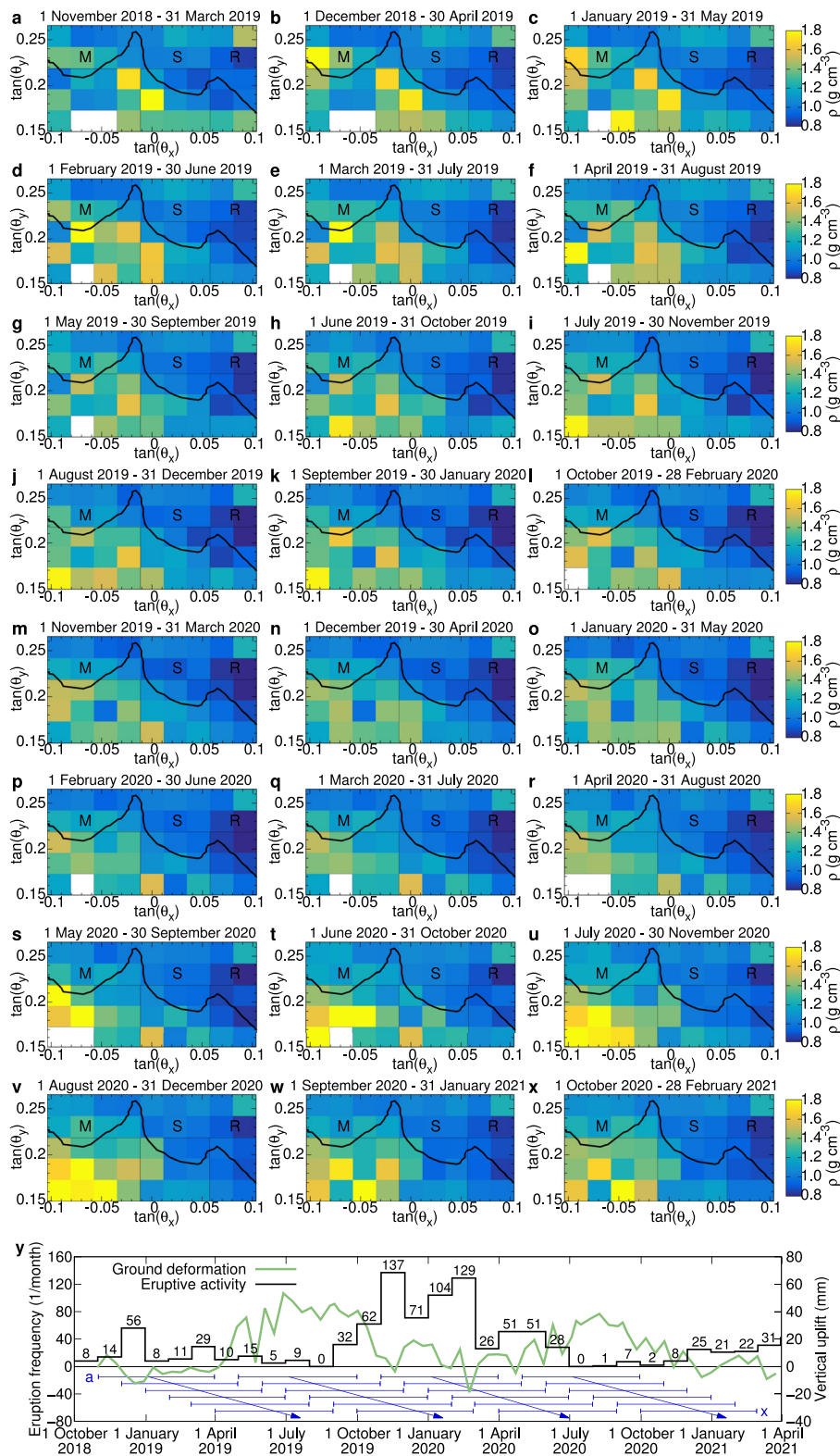
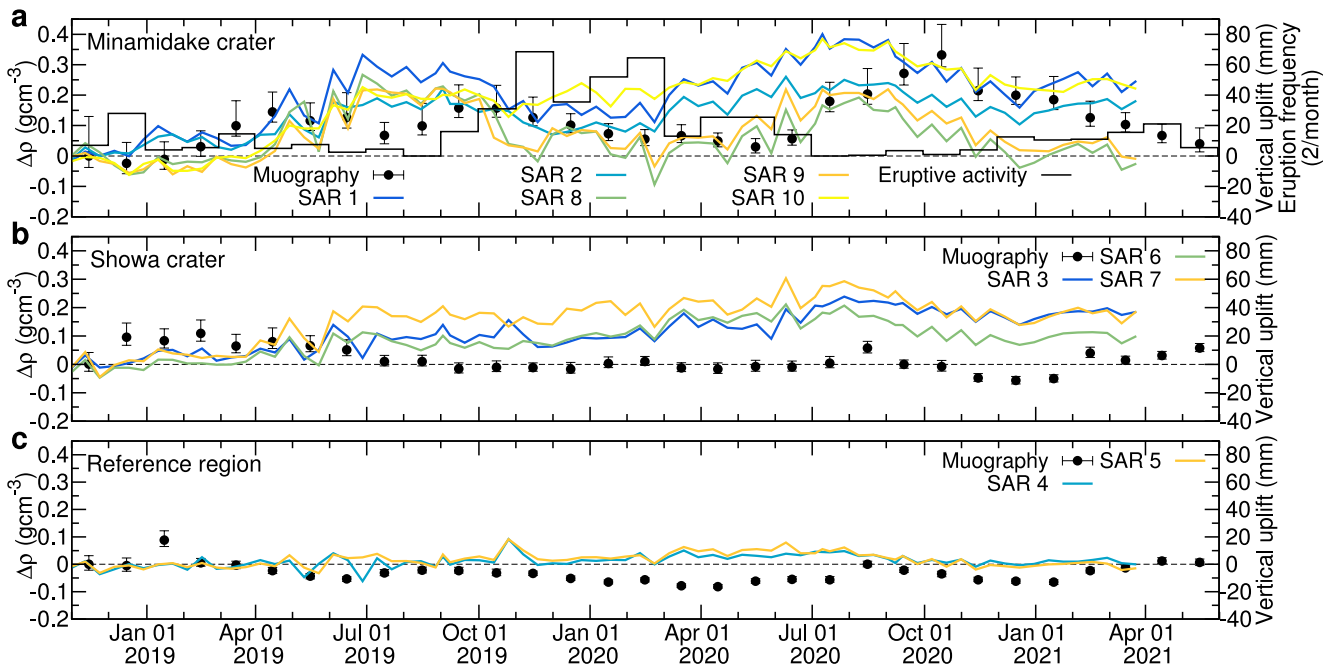


Figure 2.



**Figure 3.** Time evolution of relative averaged densities through the three regions of Sakurajima volcano. The densities (black dots) are shown with 1 standard deviation error bars from September 2018 to July 2021, relative to the averaged densities measured during the first time interval from September 1, 2018 to January 31, 2019. The dots refer to the mids of time intervals. (a) The vertical ground deformations are, respectively, shown by blue-colored, light-blue-colored, green-colored, orange-colored, and yellow-colored lines for locations 1, 2, 8, 9, and 10 at the Minamidake crater (see in Figure 1a). The eruption frequency of Minamidake crater is shown by the black histogram. (b) The vertical uplifts are, respectively, shown by blue-colored, green-colored, and orange-colored lines for locations 3, 6, and 7 at the Showa crater. (c) For the Reference region, the vertical uplifts at locations 4 and 5 are shown by blue-colored and orange-colored lines, respectively.

Vertical displacement of the volcanic edifice was determined over the same period as the muography measurements (e.g., green-colored line in Figure 2y). Displacement was determined relative to the ground level measured on October 31, 2018 at 10 locations (yellow-colored crosses in Figure 1a) using the Phased Array type C-band Synthetic Aperture Radar images acquired by Sentinel-1 (The European Space Agency, 2022) with a periodic time of 12 days. Eruption frequency (black histogram) for each crater, over the same time period, was determined from the database of Japan Meteorological Agency (2022). The Minamidake crater erupted with high frequency during periods from December 2018 to April 2019, from September 2019 to July 2020, and from December 2020 to April 2021. The eruption frequency was lower during periods from April to September 2019 and from August 2020 to January 2021. We found that ground level, averaged monthly, at the Minamidake crater (location 8 in Figure 1b and green-colored line in Figure 2y) and eruption frequencies, binned monthly, correlated inversely with a Pearson's coefficient of  $-0.718$  (Spearman's rank coefficient of  $-0.798$ ). We found moderate and weak inverse correlations for the same quantities at locations 1, 2, 3, and 9 with coefficients of  $-0.547$  ( $-0.595$ ),  $-0.509$  ( $-0.432$ ),  $-0.514$  ( $-0.421$ ), and  $-0.564$  ( $-0.685$ ), respectively. No significant correlation was found at the remaining locations. Visual inspection of Figure 2 suggests that density beneath the active craters is high during periods of low eruption frequency and upward displacement of the ground surface, and vice versa.

Arithmetic mean values of the muographically measured densities were calculated for the three regions (M, S, and R in Figure 2) to quantify their variations in relation to the eruption frequencies and ground deformation during periods of high eruption frequency and periods of quiescence. Figure 3a–3c show together: (a) 5 months average of densities with 1 standard deviation relative to the densities measured for the first time sequence from

**Figure 2.** Time-sequential density images of Sakurajima volcano. (a–x) The average density ( $\rho$ ) values are plotted for the crater region as a function of horizontal and elevation directions for periods of 5 months from November 1, 2018 to February 28, 2021. The densities were calculated for angular bins with the size of  $\Delta(\tan(\theta_x)) \times \Delta(\tan(\theta_y)) = 0.023 \times 0.023$  each. Black lines show the cross-section of craters along the AB line of Figure 1a. Black rectangular outlines designate three angular regions beneath the Minamidake crater (M), the Showa crater (S), and the Reference region (R), respectively. (y) Timelines of ground deformation (green-colored line) and eruptive frequency (black histogram) are shown for the Minamidake crater of Sakurajima volcano, Japan. Ground deformation data were recorded with interferometric synthetic aperture radar (The European Space Agency, 2022). The eruptive frequency was determined using the data from Japan Meteorological Agency (2022). Blue arrows are drawn for comparing the (a–x) images with these timelines.

September 1, 2018 to January 31, 2019 ( $\Delta\rho = \rho(t) - \rho(t_0)$ , where  $\rho(t_0)$  equals to 1.26, 1.13, and 0.99 g cm<sup>-3</sup> for the Minamidake crater, Showa crater, and Reference region, respectively); (b) the monthly number of eruptions (black histogram); and (c) the vertical ground displacement (colored lines) for each region. The relative density increased beneath the Minamidake crater (Figure 3a) throughout the periods of inflation and reduced eruption frequency. The increase of average relative densities exceeded 0.2–0.35 g cm<sup>-3</sup> which is significantly above the systematic density error of 0.06 g cm<sup>-3</sup> (see in Oláh and Tanaka (2022b) and Text S1 in Supporting Information S1). The relative densities decreased beneath the Minamidake crater during periods in which the volcanic edifice deflated and the eruption frequency increased (from November 2019 to May 2020 and from November 2020 to May 2021).

The densities beneath the dormant Showa crater (Figure 3b) slightly increased at the end of 2018 and density increase remained below 0.1 g cm<sup>-3</sup> during the observations periods. Across the Reference region (Figure 3c), the density changes were below 0.1 g cm<sup>-3</sup>.

#### 4. Discussion

We monitored the mass density changes through the upper conduit of Sakurajima volcano with muography during cyclic eruption episodes of Minamidake crater. We found that the trends in mass density were linked to trends in ground deformation and eruption frequency: the mass density increased during periods of inflation and low eruption frequency, and decreased during periods of deflation and high eruption frequency. These observed trends also correlate with other monitoring signals. During the periods from January to July 2019 and from June to November 2020 (roughly coincident with periods of high density, edifice inflation, and low eruption frequency), the time series of the vertical locations of seismic sources distributed at shallow depths underneath the Minamidake crater (middle right panel of fig. 3 in Japan Meteorological Agency (2021)) that also suggested the densification of this region. Furthermore, infrared thermal imaging revealed high-temperature regions in the Minamidake crater in August 2020 (fig. 3-1 in Japan Meteorological Agency (2020)), and glowing of Minamidake was observed in September and October 2020 (figs. 4-1 and 4-2 in Japan Meteorological Agency (2020)). During periods of low density, edifice deflation, and high eruption frequency, increased trends were observed in the sulfur dioxide discharge mass rate by JMA (upper panel of fig. 8-2 in Japan Meteorological Agency (2021)).

The increase in mass density revealed by the muography data is consistent with the formation of a dense plug of magma in the shallow plumbing system (upper ~200 m) of Minamidake crater during periods of low eruption frequency, as proposed by Gabellini et al. (2022). Upward deformation of the volcanic edifice during this period is consistent with slow upward migration of the dense, stiff plug driven by pressure from below as the conduit refills with fresh magma. We note that five highly energetic explosions occurred in June 2020 (i.e., at the start of a period of inflation) from which volcanic ejecta reached the altitude of 1.5–3.7 km above the crater rim (Japan Meteorological Agency, 2020). These events may have been associated with the onset of magma intrusion into the gas pocket. The observations of high-temperature regions and glowing material in the crater (Japan Meteorological Agency, 2020) indicate that portions of the dense, hot plug are extruded into the crater. Conversely, the decrease in mass density during periods of high eruption frequency is consistent with the presence of gas pockets in the conduit, as proposed in numerous studies (e.g., Iguchi et al., 2008; Kazahaya et al., 2016; Miwa & Toramaru, 2013; Yokoo et al., 2013). The associated deflation of the edifice may result from the cessation of recharge of magma, and the progressive outgassing of the magma within the conduit. This is consistent with the elevated sulfur dioxide discharge mass rate measured during these periods (Japan Meteorological Agency, 2020).

Concerning the Showa crater, the observed slight density increase is assumed to be a part of the plug formation process (Oláh et al., 2019) initiated at the end of 2017 by cessation of eruptive activity (Japan Meteorological Agency, 2022). Although vertical uplifting of the crater was observed from December 2018 to June 2020, no significant change was observed in the trend of mass density during this period. The minor density changes (<0.1 g cm<sup>-3</sup>) in the Reference region are consistent with its non-magmatic nature, and act as a control.

#### 5. Conclusions and Outlook

In this work, we have demonstrated that muography can complement ground surface deformation monitoring techniques via observing the evolution of mass density of magma in the shallow conduit at sufficiently high temporal and spatial resolution that changes in the eruption can be associated with changes in the state of the

magma in the shallow conduit. This has great potential for elucidating the mechanisms through which changes in eruption frequency are mediated by physical processes in the shallow conduit which, in turn, will improve conceptual, physical, and numerical models of eruptive processes. Vulcanian activity similar to that at Sakurajima is common at volcanoes worldwide, and similar conceptual models for eruption activity have been proposed (e.g., Burgisser et al., 2011; Iguchi et al., 2008; Watt et al., 2007). The model for long-period (multi-month) changes in eruptive activity that we develop here could therefore be applicable elsewhere.

## Data Availability Statement

The data sets of this study are available in a data repository of Open Science Framework (<https://doi.org/10.17605/OSF.IO/TWS4J>).

## Acknowledgments

The authors thank Christian Huber for handling our submission and two anonymous reviewers for their constructive feedback. This work was supported by the Joint Usage Research Project (JURP) of the University of Tokyo, Earthquake Research Institute (ERI) under project ID 2020-H-05, the Hungarian NKFIH research grants under identification numbers OTKA-FK-135349 and TKP2021-NKTA-10, the ELKH KT SA-88/2021 research grant; and the Ministry of Education, Culture, Sports, Science and Technology, Japan (MEXT) Integrated Program for the Next Generation Volcano Research; and the “INTENSE” H2020 MSCA RISE, GA No. 822185. G.H. is supported by the János Bolyai Research Scholarship of the HAS. The technical support provided by the members of the REGARD group is gratefully acknowledged.

## References

- Agostinelli, S., Allison, J., Amako, K., Apostolakis, J., Araujo, H., Arce, P., et al. (2003). Geant4—A simulation toolkit. *Nuclear Instruments and Methods in Physics Research Section A: Accelerators, Spectrometers, Detectors and Associated Equipment*, 506, 250–303. [https://doi.org/10.1016/S0168-9002\(03\)01368-8](https://doi.org/10.1016/S0168-9002(03)01368-8)
- Albino, F., Pinel, V., Massol, H., & Collombet, M. (2011). Conditions for detection of ground deformation induced by conduit flow and evolution. *Journal of Geophysical Research*, 116(B6), B06201. <https://doi.org/10.1029/2010jg007871>
- Ambrosino, F., Anastasio, A., Bross, A., Béné, S., Boivin, P., Bonechi, L., et al. (2015). Joint measurement of the atmospheric muon flux through the Puy de Dôme volcano with plastic scintillators and Resistive Plate Chambers detectors. *Journal of Geophysical Research: Solid Earth*, 120(11), 7290–7307. <https://doi.org/10.1002/2015jb011969>
- Biggs, J., Ebmeier, S. K., Aspinall, W. P., Lu, Z., Pritchard, M. E., Sparks, R. S. J., & Mather, T. A. (2014). Global link between deformation and volcanic eruption quantified by satellite imagery. *Nature Communications*, 5(1), 3471. <https://doi.org/10.1038/ncomms4471>
- Biggs, J., Robertson, E., & Cashman, C. (2016). The lateral extent of volcanic interactions during unrest and eruption. *Nature Geoscience*, 9(4), 308–311. <https://doi.org/10.1038/ngeo2658>
- Brenguier, F., Shapiro, N. M., Campillo, M., Ferrazzini, V., Duputel, Z., Coutant, O., & Nercessian, A. (2008). Towards forecasting volcanic eruptions using seismic noise. *Nature Geoscience*, 1(2), 126–130. <https://doi.org/10.1038/ngeo104>
- Burgisser, A., Arbaret, L., Druitt, T. H., & Giachetti, T. (2011). Pre-explosive conduit conditions of the 1997 Vulcanian explosions at Soufrière Hills Volcano, Montserrat: II. Overpressure and depth distributions. *Journal of Volcanology and Geothermal Research*, 199(3–4), 193–205. <https://doi.org/10.1016/j.jvolgeores.2010.11.014>
- Caricchi, L., Blundy, J., Simpson, G., & Pinel, V. (2014). Frequency and magnitude of volcanic eruptions controlled by magma injection and buoyancy. *Nature Geoscience*, 7(2), 126–130. <https://doi.org/10.1038/ngeo2041>
- Chouet, B. (1996). Long-period volcano seismicity: Its source and use in eruption forecasting. *Nature*, 380(6572), 309–316. <https://doi.org/10.1038/380309a0>
- Dempsey, D. E., Cronin, S. J., Mei, S., & Kempa-Liehr, A. W. (2020). Automatic precursor recognition and real-time forecasting of sudden explosive volcanic eruptions at Whakaari, New Zealand. *Nature Communications*, 11(1), 3562. <https://doi.org/10.1038/s41467-020-17375-2>
- Fischer, T. P., Morrissey, M. M., Marta Lucía Calvache, V., Diego Gómez, M., Roberto Torres, C., Stix, J., & Williams, S. N. (1994). Correlations between SO<sub>2</sub> flux and long-period seismicity at Galeras volcano. *Nature*, 368(6467), 135–137. <https://doi.org/10.1038/368135a0>
- Francis, P., Thorpe, R., Brown, G., & Glasscock, J. (1980). Pyroclastic sulphur eruption at Poas volcano, Costa Rica. *Nature*, 283(5749), 754–756. <https://doi.org/10.1038/283754a0>
- Gabellini, P., Cioni, R., Geshi, N., Pistolesi, M., Miwa, T., Lacanna, G., & Ripepe, M. (2022). Eruptive dynamics and fragmentation mechanisms during cyclic Vulcanian activity at Sakurajima volcano (Japan): Insights from ash texture analysis. *Journal of Volcanology and Geothermal Research*, 428, 107582. <https://doi.org/10.1016/j.jvolgeores.2022.107582>
- Geological Survey of Japan. (2013). Geological map of Sakurajima Volcano. Retrieved from [https://gbank.gsj.jp/volcano/Act\\_Vol/sakurajima/text/eng/exp01-1e.html](https://gbank.gsj.jp/volcano/Act_Vol/sakurajima/text/eng/exp01-1e.html)
- Gibert, D., de Bremond d’Ars, J., Carls, B., Deroussi, S., Ianigro, J.-C., Jessop, D. E., et al. (2022). Observation of the dynamics of hydrothermal activity in La Soufrière de Guadeloupe volcano with joint muography, gravimetry, electrical resistivity tomography, seismic and temperature monitoring. *Geophysical Monograph Series*, 270, 55–73. <https://doi.org/10.1002/9781119722748.ch5>
- Groom, D. E., Mokhov, N. V., & Striganov, S. I. (2002). Muon stopping power and range tables 10 MeV–100 TeV. *Atomic Data and Nuclear Data Tables*, 76(2), 183–356. <https://doi.org/10.1006/adnd.2001.0861>
- Iguchi, M., Yakiwara, H., Tameguri, T., Hendrasto, M., & Hirabayashi, J. (2008). Mechanism of explosive eruption revealed by geophysical observations at the Sakurajima, Suwanosejima and Semeru volcanoes. *Journal of Volcanology and Geothermal Research*, 178, 1–9. <https://doi.org/10.1016/j.jvolgeores.2007.10.010>
- Japan Meteorological Agency. (2020). Report of 147th coordinating committee of prediction of volcanic eruption. Retrieved from [https://www.data.jma.go.jp/svd/vois/data/tokyo/STOCK/kaisetsu/CCPVE/shiryo/147/147\\_2-1.pdf](https://www.data.jma.go.jp/svd/vois/data/tokyo/STOCK/kaisetsu/CCPVE/shiryo/147/147_2-1.pdf)
- Japan Meteorological Agency. (2021). Report of 149th coordinating committee of prediction of volcanic eruption. Retrieved from [https://www.data.jma.go.jp/svd/vois/data/tokyo/STOCK/kaisetsu/CCPVE/shiryo/149/149\\_2-1.pdf](https://www.data.jma.go.jp/svd/vois/data/tokyo/STOCK/kaisetsu/CCPVE/shiryo/149/149_2-1.pdf)
- Japan Meteorological Agency. (2022). Monthly data of Sakurajima eruptions. Retrieved from [https://www.jma-net.go.jp/kagoshima/vol/data/skr\\_erp\\_num.html](https://www.jma-net.go.jp/kagoshima/vol/data/skr_erp_num.html)
- Kazahaya, R., Shinohara, H., Mori, T., Iguchi, M., & Yokoo, A. (2016). Pre-eruptive inflation caused by gas accumulation: Insight from detailed gas flux variation at Sakurajima volcano, Japan. *Geophysical Research Letters*, 43(21), 11219–11225. <https://doi.org/10.1002/2016gl070727>
- Leone, G., Tanaka, H. K. M., Holma, M., Kuusiniemi, P., Varga, D., Oláh, L., et al. (2021). Muography as a new complementary tool in monitoring volcanic hazard: Implications for early warning systems. *Proceedings of the Royal Society A*, 477(2255), 20210320. <https://doi.org/10.1098/rspa.2021.0320>
- Lipari, P., & Stanev, T. (1991). Propagation of multi-TeV muons. *Physical Review D*, 44(11), 3543–3554. <https://doi.org/10.1103/physrevd.44.3543>
- Londoño, J. M., & Kumagai, H. (2018). 4D seismic tomography of Nevado del Ruiz Volcano, Colombia, 2000–2016. *Journal of Volcanology and Geothermal Research*, 358, 105–123. <https://doi.org/10.1016/j.jvolgeores.2018.02.015>



- Lo Presti, D., Gallo, G., Bonanno, D. L., Bonanno, G., Ferlito, C., La Rocca, P., et al. (2022). Three years of muography at Mount Etna, Italy: Results and interpretation. *Geophysical Monograph Series*, 270, 93–108. <https://doi.org/10.1002/9781119722748.ch7>
- Macedonio, G., Saracino, G., Ambrosino, F., Baccani, G., Bonechi, L., Bross, A., et al. (2022). Muography of the volcanic structure of the Summit of Vesuvius. *Geophysical Monograph Series*, 270, 123–136. <https://doi.org/10.1002/9781119722748.ch9>
- Massonnet, D., Briole, P., & Arnaud, A. (1995). Deflation of Mount Etna monitored by spaceborne radar interferometry. *Nature*, 375(6532), 567–570. <https://doi.org/10.1038/375567a0>
- Melnik, O., & Sparks, R. S. J. (2002). Dynamics of magma ascent and lava extrusion at Soufrière Hills Volcano, Montserrat. *Geological Society, London, Memoirs*, 21(1), 153–171. <https://doi.org/10.1144/gsl.mem.2002.021.01.07>
- Miwa, T., & Toramaru, A. (2013). Conduit process in vulcanian eruptions at Sakurajima volcano, Japan: Inference from comparison of volcanic ash with pressure wave and seismic data. *Bulletin of Volcanology*, 75(1), 1–13. <https://doi.org/10.1007/s00445-012-0685-y>
- Miyamoto, S., Nagahara, S., Morishima, K., Nakano, T., Koyama, M., & Suzuki, Y. (2022). A muographic study of a scoria cone from 11 directions using nuclear emulsion cloud chambers. *Geoscientific Instrumentation, Methods and Data Systems*, 11(1), 127–147. <https://doi.org/10.5194/gi-11-127-2022>
- Nishiyama, R., Tanaka, Y., Okubo, S., Oshima, H., Tanaka, H. K. M., & Maekawa, T. (2014). Integrated processing of muon radiography and gravity anomaly data toward the realization of high-resolution 3-D density structural analysis of volcanoes: Case study of Showa-Shinzan lava dome, Usu, Japan. *Journal of Geophysical Research: Solid Earth*, 119(1), 699–710. <https://doi.org/10.1002/2013jb010234>
- Nomura, Y., Nemoto, M., Hayashi, N., Hanaoka, S., Murata, M., Yoshikawa, T., et al. (2020). Pilot study of eruption forecasting with muography using convolutional neural network. *Scientific Reports*, 10(1), 5272. <https://doi.org/10.1038/s41598-020-62342-y>
- Oláh, L., & Tanaka, H. K. M. (2022a). Machine learning with muographic images as input: An application to volcano eruption forecasting. *Geophysical Monograph Series*, 270, 43–54. <https://doi.org/10.1002/9781119722748.ch4>
- Oláh, L., & Tanaka, H. K. M. (2022b). Muography of magma intrusion beneath the active craters of Sakurajima volcano. *Geophysical Monograph Series*, 270, 109–122. <https://doi.org/10.1002/9781119722748.ch8>
- Oláh, L., Tanaka, H. K. M., & Hamar, G. (2021). Muographic monitoring of hydrogeomorphic changes induced by post-eruptive lahars and erosion of Sakurajima volcano. *Scientific Reports*, 11(1), 17729. <https://doi.org/10.1038/s41598-021-96947-8>
- Oláh, L., Tanaka, H. K. M., Ohminato, T., Hamar, G., & Varga, D. (2019). Plug formation imaged beneath the active craters of Sakurajima Volcano with muography. *Geophysical Research Letters*, 46(17–18), 10417–10424. <https://doi.org/10.1029/2019gl084784>
- Oláh, L., Tanaka, H. K. M., Ohminato, T., & Varga, D. (2018). High-definition and low-noise muography of the Sakurajima volcano with gaseous tracking detectors. *Scientific Reports*, 8(1), 3207. <https://doi.org/10.1038/s41598-018-21423-9>
- Patané, D., DeGori, P., Chiarabba, C., & Bonaccorso, A. (2003). Magma ascent and the pressurization of Mount Etna's volcanic system. *Science*, 299(5615), 2061–2063. <https://doi.org/10.1126/science.1080653>
- Pinel, V., Poland, M. P., & Hooper, A. (2014). Volcanology: Lessons learned from Synthetic Aperture Radar imagery. *Journal of Volcanology and Geothermal Research*, 289, 81–113. <https://doi.org/10.1016/j.jvolgeores.2014.10.010>
- Poland, M. P., & Anderson, K. R. (2020). Partly cloudy with a chance of lava flows: Forecasting volcanic eruptions in the twenty-first century. *Journal of Geophysical Research: Solid Earth*, 125(1), e2018JB016974. <https://doi.org/10.1029/2018jb016974>
- Poland, M. P., & Carbone, D. (2016). Insights into shallow magmatic processes at Kilauea volcano, Hawai'i, from a multiyear continuous gravity time series. *Journal of Geophysical Research: Solid Earth*, 121(7), 5477–5492. <https://doi.org/10.1002/2016jb013057>
- Sano, Y., Kagoshima, T., Takahata, N., Nishio, Y., Roulleau, E., Pinti, D. L., & Fischer, T. P. (2015). Ten-year helium anomaly prior to the 2014 Mt Ontake eruption. *Scientific Reports*, 5(1), 13069. <https://doi.org/10.1038/srep13069>
- Sparks, R. S. J. (2003). Forecasting volcanic eruptions. *Earth and Planetary Science Letters*, 210(1–2), 1–15. [https://doi.org/10.1016/s0012-821x\(03\)00124-9](https://doi.org/10.1016/s0012-821x(03)00124-9)
- Syahbana, D. K., Kasbani, K., Suantika, G., Prambada, O., Andreas, A. S., Saing, U. B., et al. (2019). The 2017–19 activity at Mount Agung in Bali (Indonesia): Intense unrest, monitoring, crisis response, evacuation, and eruption. *Scientific Reports*, 9(1), 8848. <https://doi.org/10.1038/s41598-019-45295-9>
- Tanaka, H. K. M., Kusagaya, T., & Shinohara, H. (2014). Radiographic visualization of magma dynamics in an erupting volcano. *Nature Communications*, 5(1), 3381. <https://doi.org/10.1038/ncomms4381>
- Tanaka, H. K. M., Nakano, T., Takahashi, S., Yoshida, J., Takeo, M., Oikawa, J., et al. (2007). High resolution imaging in the inhomogeneous crust with cosmic-ray muon radiography: The density structure below the volcanic crater floor of Mt. Asama, Japan. *Earth and Planetary Science Letters*, 263(1–2), 104–113. <https://doi.org/10.1016/j.epsl.2007.09.001>
- Tanaka, H. K. M., Uchida, T., Tanaka, M., Shinohara, H., & Taira, H. (2009). Cosmic-ray muon imaging of magma in conduit: Degassing process of Satsuma-Iwojima Volcano, Japan. *Geophysical Research Letters*, 36(1), L01304. <https://doi.org/10.1029/2008gl036451>
- Tang, A., Horton-Smith, G., Kudryavtsev, V. A., & Tonazzo, A. (2006). Muon simulations for Super-Kamiokande, KamLAND, and CHOOZ. *Physical Review D*, 74(5), 053007. <https://doi.org/10.1103/physrevd.74.053007>
- The European Space Agency. (2022). SAR Instrument. Retrieved from <https://sentinels.copernicus.eu/web/sentinel/technical-guides/sentinel-1-sar/sar-instrument>
- Tioukov, V., Giudicepietro, F., Macedonio, G., Calvari, S., Di Traglia, F., Fornaciai, A., & Favalli, M. (2022). Structure of the shallow supply system at Stromboli Volcano, Italy, through integration of muography, digital elevation models, seismicity, and ground deformation data. *Geophysical Monograph Series*, 270, 75–91. <https://doi.org/10.1002/9781119722748.ch6>
- Varga, D., Hamar, G., Balogh, S., Gera, A., Nyitrai, G., & Surányi, G. (2022). Construction and readout systems for gaseous muography detectors. *Journal of the Indian Institute of Science*, JAIS-307. <https://doi.org/10.31526/jais.2022.307>
- Varga, D., Nyitrai, G., Hamar, G., Galgóczi, G., Oláh, L., Tanaka, H. K. M., & Ohminato, T. (2020). Detector developments for high performance Muography applications. *Nuclear Instruments and Methods in Physics Research Section A: Accelerators, Spectrometers, Detectors and Associated Equipment*, 958, 162236. <https://doi.org/10.1016/j.nima.2019.05.077>
- Watt, S. F. L., Mather, T. A., & Pyle, D. M. (2007). Vulcanian explosion cycles: Patterns and predictability. *Geology*, 35(9), 839–842. <https://doi.org/10.1130/g23562a.1>
- Werner, C., Kelly, P. J., Doukas, M., Lopez, T., Pfeffer, M., McGimsey, R., & Neal, C. (2013). Degassing of CO<sub>2</sub>, SO<sub>2</sub>, and H<sub>2</sub>S associated with the 2009 eruption of Redoubt Volcano, Alaska. *Journal of Volcanology and Geothermal Research*, 259, 270–284. <https://doi.org/10.1016/j.jvolgeores.2012.04.012>
- Woods, A. W., & Koyaguchi, T. (1994). Transitions between explosive and effusive eruptions of silicic magmas. *Nature*, 370(6491), 641–644. <https://doi.org/10.1038/370641a0>
- Yokoo, A., Iguchi, M., Tameguri, T., & Yamamoto, K. (2013). Processes prior to outbursts of Vulcanian eruption at Showa crater of Sakurajima Volcano. *Bulletin of the Volcanological Society of Japan*, 58, 163–181. [https://doi.org/10.18940/kazan.58.1\\_163](https://doi.org/10.18940/kazan.58.1_163)